A magnetotelluric profile across the KTB surrounding: 2-D and 3-D modeling results

Markus Eisel[1], Josef Pek[2], Václav Červ[3], Volker Haak[4]

Introduction

The interpretation of MT data collected in the surrounding of the German Continental Deep Drilling Project (Eisel, 1995), (Červ et al., 93 a), (Červ et al., 93 b), (Eisel and Haak, 1998) (and references herein) revealed a number of interesting findings – but also posed a number of unanswered questions. Most of the authors mentioned above suggested a conductive structure at mid-crustal depth: The "10-km–conductor". Eisel (1990) and Tauber (1993) developed detailed images of this large scale structure and a slightly modified model can be found in Eisel & Haak (1998). The second dominant feature of MT data from this region is the high anisotropy of MT sounding curves which is interpreted by an electrically highly anisotropic upper to middle crust (Eisel and Haak, 1998). Despite the detailed models of the separate structures the combination of them could not be modeled to satisfaction so far, namely because of the restricted amount and quality of data.

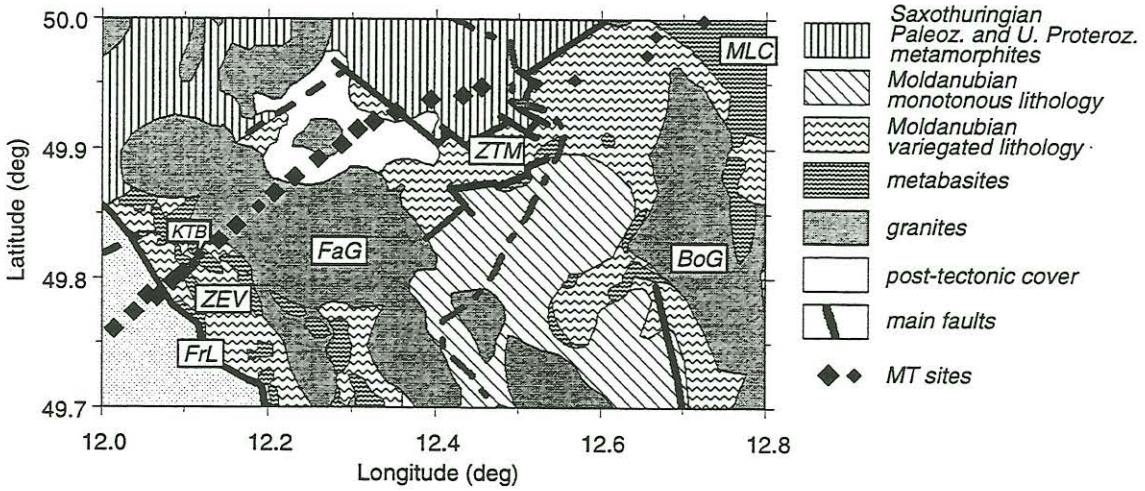

Figure 1: Schematic geological map of the survey area and locations of the MT soundings (small diamonds indicate sites unprocessed so far). Abbreviations: FrL–Franconian Line, ZEV–Zone of Erbendorf and Vohenstrauß, FaG–Falkenberg Granite, ZTM–Zone of Tirschenreuth and Mähring, BoG–Bor Granitic Massif, MLC–Mariánské Lázně Ultrabasic Complex, KTB–KTB drill site.

In order to find solutions for the superposition of the structures and to answer questions about the continuation of the anisotropic region towards the north-east MT measurements were carried out along a profile from west of the Franconian Line across the ZEV and the Czech-German border into the region of Mariánské Lázně (Marienbad). This contribution presents the data collected and discusses different approaches to model the MT data from this region of a highly complex crust. In order to keep the paper short we will focus on the modeling sections and only briefly discuss the problems of processing the data.

Geology, Site locations and instrumentation

The KTB drill site is located on the western border of the Bohemian Massif, which is the largest outcrop of basement rocks in Central Europe. In particular the drill site is on a distinct gneiss-metabasite unit called the Zone of Erbendorf-Vohenstrauß(ZEV). While this ZEV-unit was modeled in the pre-drilling

[1]College of Oceanic and Atmospheric Sciences, Oregon State University, Corvallis, OR, 97331, e-mail: eisel@oce.orst.edu
[2]Geophysical Institute, Academy of Sciences of the CR, Bocni II 14131 Prague 4-Sporilov, e-mail: jpk@ig,cas,cz
[3]Geophysical Institute, Academy of Sciences of the CR, Bocni II 14131 Prague 4-Sporilov, e-mail: vcv@ig,cas,cz
[4]GeoForschungsZentrum Potsdam, Telegrafenberg, 14473 Potsdam, e-mail: vhaak@gfz-potsdam.de

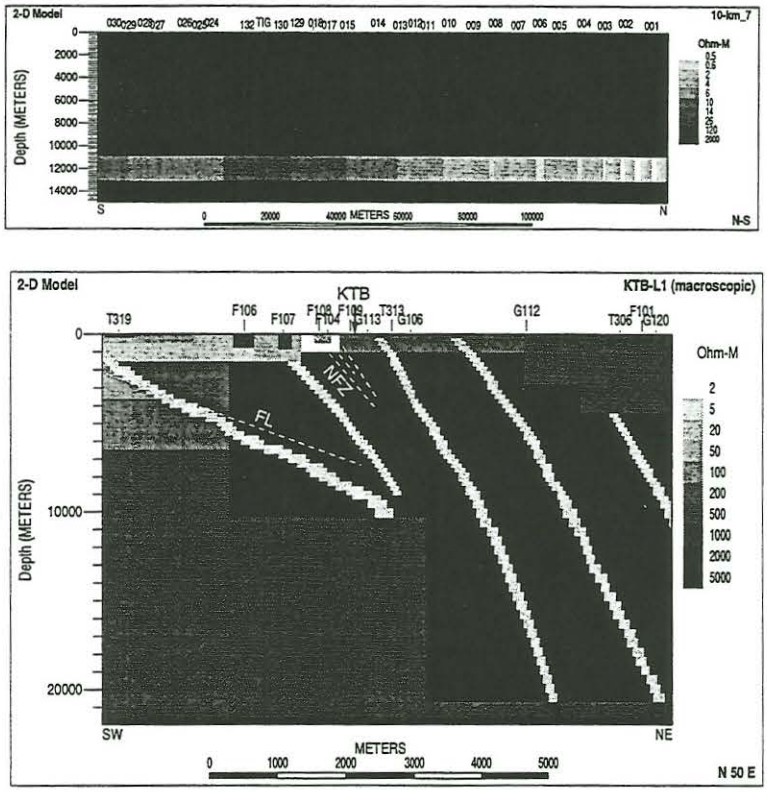

Figure 2: Top: The model of the regional "10-km-conductor", a conductive layer at 11 km depth with E-W striking segments yielding a conductance gradient from N to S. Bottom: The local model along a SW-NE section across the ZEV. Conductive, sub-vertical dikes within a resistive host-rock produce the observed high anisotropy of MT impedances.

era as a thin klippe lying on metamorphic Moldanubian and Saxothuringian rocks, the model changed in the post-drilling era - as a result of numerous investigations of the then available third dimension - to a stacked and repeated pile of vertically rotated rocks along graphitized shear-zones. In the west the NW-SE striking Franconian Lineament (FL) separates the rocks of the ZEV in the east from post tectonic sediments in the west. The Falkenberg Granite builds the eastern boundary of the narrow ZEV complex. Fig. 1 shows the main geological units of the area.

The MT soundings were carried out along a profile running in SW-NE direction. This direction is perpendicular to the strike of the FL and the anisotropic structure suggested by the model of Eisel (1995). Site spacing is approximately 2 km with higher coverage in the ZEV region and totals to 26 sites. The western most sites are about 6 km west of the FL. To account for an observed change in direction of the anisotropy (Červ et al., 93 b) the direction of the profile changed to a WSW-ENE direction in the eastern part of the profile.

The measurements were made with the KMT-systems of the GFZ which consist of an induction coil triple and a 6-channel data-logger with an external hard-disk as mass-storage. Up to ten of these instruments were recording simultaneously, time-synchronized via GPS-receivers, at 20 Hz digitization rate. The western most site (REF) served as a reference site for the survey and recorded during the whole survey period of 30 days. AMT data were recorded at each site using the SPAM Mark III system. This data is not part of this paper.

Previous results of MT data interpretation

In this section we briefly want to describe two major results derived from MT data interpretation so far. There seems to be a general agreement about the existence of of a mid-crustal conductive structure of regional scale. Such a structure was proposed already in early interpretations and was refined in later studies (Eisel, 1990), (Tauber, 1993). This regional model is mainly based on the interpretation of induction vectors (IV) measured in the vicinity of the KTB and along a 150 km NS profile from the Vogtland to the Bavarian Forest (Tauber, 1993). A refined version of this model is shown in Fig. 2 (Eisel and Haak, 1998). It consists of a conductive layer at 10 km depth within a resistive background. The layer itself is divided into EW striking blocks yielding a decreasing conductance from north to south.

The second model is of local scale and covers a SW-NE cross section of the ZEV just south of the KTB-location. The striking feature of the data from this region is the extremely high anisotropy of the

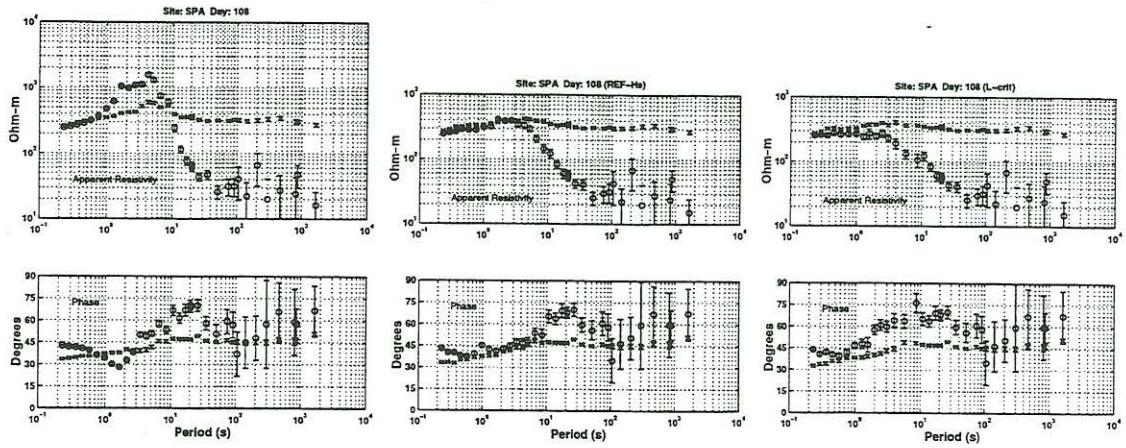

Figure 3: Apparent resistivity and phase curves from different processing approaches for site SPA, day 108. Left panel: Unconstrained multiple station processing (array size: 6 stations). Middle: Results from a multiple station processing using the H-fields from REF as an initial reference field. Right: Applying the 0-1-weight vector from Fig. 4 to the data. Only 265 sets out of 4498 were used in the period band 0.8 - 25 s.

MT impedances. Strike directions determined from MT data are sub-parallel to the FL. The minor axis of anisotropy points in this direction (NW-SE) while the major axis is directed NE-SW. The discrepancy between the very high anisotropy of the MT impedances on the one hand and the almost neglectable anisotropy measured on rock samples from the drill holes suggested that the anisotropy is caused by macroscopic structures rather than by rock-intrinsic properties. Fig. 2 shows the model of conductive sub-vertical dikes within a resistive host-rock derived from the MT impedances measured along a profile across the ZEV (Eisel, 1995).

Each model considered by itself gives a reasonable interpretation of the data it is based on. The problems arise as soon as one tries to superimpose the two models. Incorporating a conductive layer at 11 km depth into the dike model deteriorates the fit of the impedance data. On the other hand an additive superposition of the IV from the two models is in agreement with the observed IV (Eisel, 1995). The restricted amount of data and the poor data quality led to the proposal of new MT measurements which hopefully can solve these questions.

Data acquisition and data processing

Ten KMT-systems were used for the measurements, one of which served as a reference station for the whole survey. Average recording time at each of the 25 remaining sites was 5 days with small gaps due to battery and hard-disk changes. In general, up to seven systems were recording simultaneously, all synchronized via GPS. For processing this data we used the multiple-station-processing by Egbert (1997), an approach which accounts for the multivariate character of such array data. In addition to improved MT transfer functions it provides diagnostics on possible coherent noise in the data, which can bias the results and lead to misinterpretations.

As we learned during this process, coherent noise was present at all sites of the array, even though the western sites were affected less than those to the east. The left panel of Fig. 3 gives an example of the bias effect of coherent noise: An upward bias of apparent resistivity curves in the period range 1 - 20 s, the so-called *dead band*.

More detailed investigations revealed that there is a substantial change of signal/noise ratio as a function of time and therefore a variation of the transfer functions with time. To discriminate between segments which are not or only little affected by coherent noise and those which are strongly disturbed the following procedure was developed: First, a set of 'standard' transfer functions (impedances and vertical magnetic field TFs) of the reference site REF was defined by selecting data segments which obviously

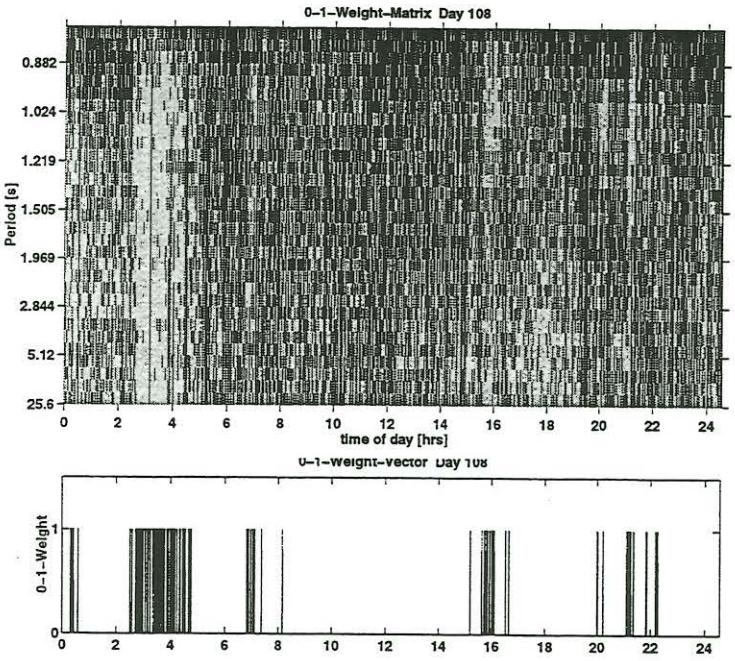

Figure 4: Top: Matrix of 0- (reject) 1- (accept) weights for the 4498 time windows and 32 periods of (0.8 - 26 s) for 24 hours of data from day 108. The weights are calculated from the residual between the data-vector of each time/frequency element of the reference site and it's projection into the space defined by a set of standard transfer functions (refer to text for more details). Bottom: 0-1-weight-vector derived from summation over the frequencies in the matrix above. These weights define which time-sections are accepted for stacking in the processing.

did not show bias effects. Extending this matrix to the magnetic field TFs yields

$$\hat{V} = \begin{pmatrix} 1 & 0 \\ 0 & 1 \\ Z_{zx} & Z_{zy} \\ Z_{xx} & Z_{xy} \\ Z_{yx} & Z_{yy} \end{pmatrix},$$

a matrix whose columns span the space in which the data vector $X_i = (H_x, H_y, H_z, E_x, E_y)$ of an undisturbed time segment i would lie. The Z_{ij} are the 'standard' TFs of REF.

A measure for the deviation of X_i from this space is the residual

$$\vec{X}_{R,i} = \vec{X}_i - \vec{X}_{P,i}$$

where $\vec{X}_{P,i}$ is the projection of X_i into $\hat{V}$.

$$\vec{X}_{P,i} = [\hat{V} \cdot (\hat{V}^T \cdot \hat{V})^{-1} \cdot \hat{V}^T] \cdot \vec{X}_i$$

Applying this to all time segments (at 4 Hz sampling rate, a window length of 128 points and 24 h of continuous data we look at 4498 segments and 32 periods) yields a weight matrix $\hat{L}$ whose elements are given by

$$L_{j,k} = \begin{cases} 1 & \forall \quad ||\vec{X}_{R,j,k}||/(||H_x|| + ||H_y||) < 0.1 \\ 0 & \forall \quad ||\vec{X}_{R,j,k}||/(||H_x|| + ||H_y||) \geq 0.1 \end{cases}$$

This matrix is displayed in Fig. 4 (top). In a first step this matrix was applied to the total set of time segments and periods but didn't give a satisfying result. In a second step, we calculated the sum over all columns (periods) yielding the weight vector $\hat{LL}$ shown in Fig. 4, bottom.

$$LL_k = \begin{cases} 1 & \forall \quad \sum_m L_{k,m} > 30 \\ 0 & \forall \quad \sum_m L_{k,m} \leq 30 \end{cases}, \quad k = 1, ..., 4498$$

These weights now define which time segments are included in the robust multiple station processing. Fig. 3, (right) shows, as an example, the final apparent resistivity and phase curves for site SPA, day 108, derived using the procedure described above. A clear improvement over processing results from different approaches (left panels) is visible.

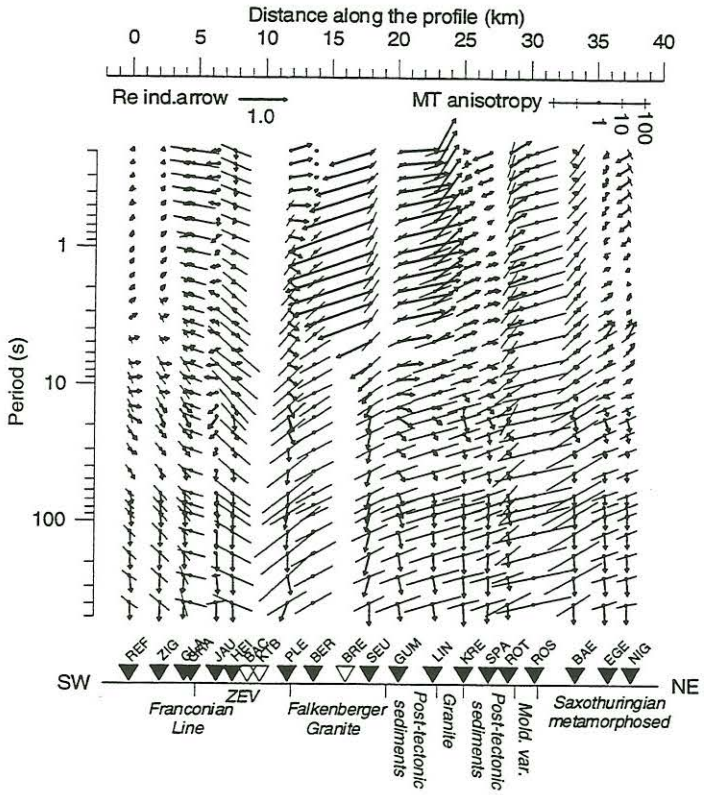

Figure 5: Real IV (bold arrows) and Swift's principal directions (thin lines indicate the direction of the maximum impedance, their length is proportional to the log of the MT anisotropy) for the individual MT sites and for all periods. At the bottom, the MT sites along the profile are shown along with their position with respect to the main geological features of the region. Empty triangles are for sites unprocessed so far.

Data inspection and analysis

At present, most of the data have been processed in the period range 0.2 to 2000 s, along the German section of the profile. The MT curves clearly reflect the geological differentiation along the profile, indicating three main sub-provinces with distinct features:

- Within the Permo-Mesozoic sediments W of the Franconian Line relatively low resistivities with low to moderate MT anisotropies at longer periods only are observed (sites REF, ZIG, GLA and GRA, see Fig. 5).

- The sites JAU and HEI,within the ZEV complex close to the Franconian Line (Fig. 5), seem to be affected by a large local distorting effect, manifested even by a local reversal of short-period real IV between those sites. A highly anomalous character of this zone is further supported by a large local increase of both the skew and regional skew between the sites GRA and HEI. Site PLE, close to the eastern margin of the ZEV, fits well into the general MT image of the ZEV, with a high NW-SE (minimum impedances) anisotropy of the MT curves and a typical course of the azimuths of the real IV from the NE for short periods towards the S observed regionally for periods longer than about 30 s.

- MT curves east of the ZEV seem to display a rather high degree of conformity. Except at short periods, where various effects of near-surface heterogeneities affect the data, the curves show a quasi-uniform anisotropy with minor impedances directed about N20°W. This differs substantially from the western section of the profile, where the principal directions are governed by the strike of the local geology, about N40°W. Another common feature of the curves east of PLE is their shape, which fits the general pattern of typical MT curves both from the ZEV (Eisel, 1995) and from West Bohemia (Červ et al., 1997). The yx-apparent resistivity curves are almost constant, without indicating any deeper conductive structures, whereas the xy-curves always drop substantially within the period range between 1 to 20 s. The phases show a corresponding shape. The left-hand panel of Fig. 6 clearly demonstrates this divergence by showing all the data in one graph. The resistivity curves were shifted to match the median resistivity at 10 s period. The right-hand panel of Fig. 6 shows the MT curves for site SPA, which is representative for the above cluster, and 1-D models of the two modes to display the degree of crustal anisotropy required to fit the observed curve splitting.

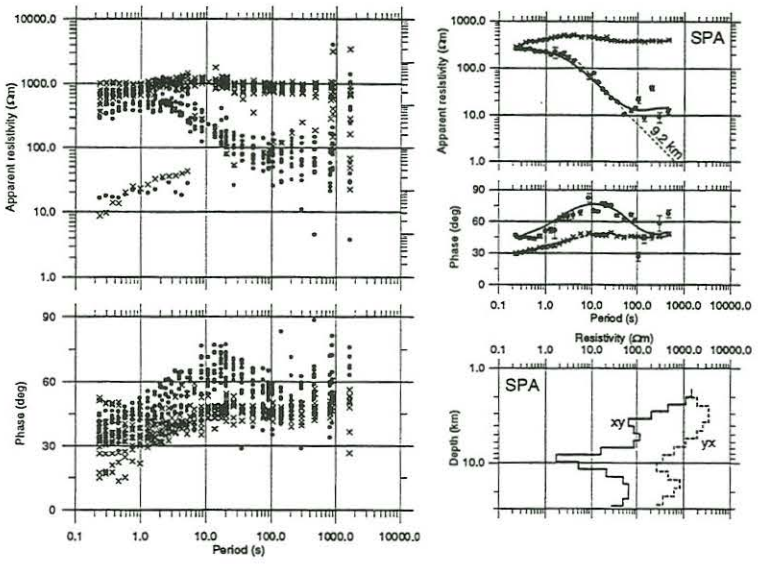

Figure 6: Left panel—Apparent resistivities (top) and phases (bottom) of xy (full circles) and yx (crosses) curves for all MT sites in the central and NE section of the profile (sites E of PLE). The apparent resistivities are shifted to their median value at the period of 10 s. Right panel—1-D inversion of the xy (full circles) and yx (crosses) MT data at the site SPA. The 1-D resistivity models for the individual modes are shown in the bottom figure, the corresponding model curves are compared with the data in the top two figures. A simple asymptotic estimate from the xy apparent resistivity curve indicates the depth to the top of a conductor at about 9 km.

The directional properties of the data can be summarized as follows:

a) In the SW part of the profile, specifically W of BRE, Swift's principal direction is dominated by the geological strike of the ZEV subregion and the FL. Exceptions are sites influenced by evidently large distortions near the Franconian Line (GRA, JAU, HEI), which must be treated individually.

b) For the sites E of BRE, the MT data show an almost homogeneous direction close to N70°E (major impedances) for periods longer than a few seconds.

c) Long period real IV are almost uniformly directed to the S, independently of their position with respect to the geological units.

d) The E-W component of the IV is dominating at short periods all along the profile. Exceptions are HEI for the shortest period, and LIN and ROS, with evident local deflections towards the N.

e) In spite of more dynamics in the short-period IV, MT directions at long periods agree well with the directions of the IV at short periods. For longer periods, the MT impedances do not follow the IV, and the directions of the telluric field on the one hand and the magnetic field on the other seem to be dominated by different structures.

The character of the MT data, in particular along the NE section of the profile, would qualitatively indicate a possibly composite nature of the structure studied, with a laterally quasi-uniform inductive zone and local galvanic distortions involved. Unfortunately, the quantitative analysis of the MT decomposition parameters did not provide clear indications as to a composite model of the structure. We used the techniques of Groom & Bailey (1989) and Bahr (1991) to compute both the single period and interval estimates of the decomposition parameters for a 3-D local/2-D regional composite model scheme. Estimates of the regional strike direction are relatively consistent only within the period range from about 3 to 100 s, indicating a regional direction close to -10° with rather large scatter of the individual estimates. Other distortion parameters show strong scatter and cannot prove the frequency-independence of the decomposition parameters.

The failure of the decomposition schemes reflects what the above qualitative discussion of the the MT data already suggested: Apart from the ZEV, at least three further major structures show up in the MT characteristics, (i) the large scale regional E-W striking structure causing the south pointing IV at periods longer than about 30 s, (ii) the close to 1-D structures at shallow depths west of the Franconian Line, and, with increasing period, the contact zone along the Franconian Line itself, and (iii) the structure east of the ZEV above the regional conductor and below the small scale local near-surface heterogeneities. This structure, striking roughly N20°W, dominates the IV at periods 0.2 to 5 s and the telluric directions at periods longer than 10 s. East of the ZEV, the preferred strike of the main geological structures gradually

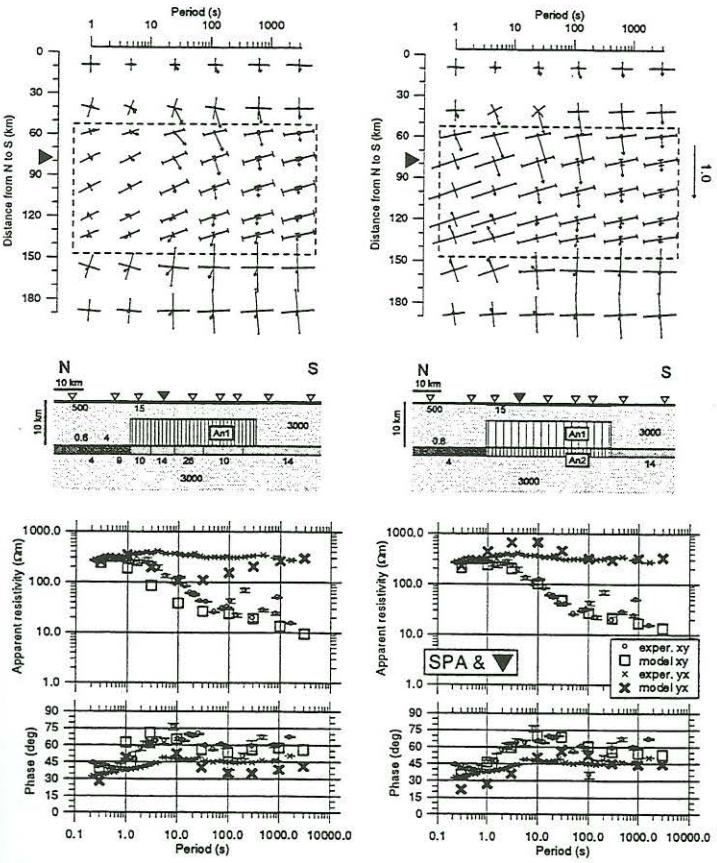

Figure 7: Results of the 2-D modeling of the interaction between the mid-crustal conductor and an anisotropic crustal block. Left panels: Model with the anisotropic block An1 overlying the conductor. An1 is a horizontally anisotropic structure with $\varrho_{min}/\varrho_{max}$ = 1.5/3000 Ωm and the direction of the best conductivity. Top: plan view of the real IV and MT impedances (representation according to (Siemon, 1991)) at selected sites for six periods. The dashed rectangle indicates the extent of the anisotropic block. Center: N-S cross-section of the model with resistivities in Ωm. Triangles on the surface mark sites for which the IV and impedances are plotted in the top panel. Bottom: Comparison of apparent resistivity and phase curves from site SPA and the model site marked by the filled triangle. Right panels: Same figures for a model with the anisotropic structure An1 ∪ An2 penetrating through the mid-crustal conductor. An1 and An2 are horizontally anisotropic blocks with $\varrho_{min}/\varrho_{max}$ = 100/3000 Ωm and 1.5/300 Ωm, respectively, and both with $\alpha_{min} = 70°$ with respect to the structural strike.

tends closer to the N. Thus, the continuity of the anisotropic pattern of the MT curves from the ZEV towards the east, accompanied by a systematic deflection of the telluric directions conforming to the variations of the geological strike, could support the hypothesis that the above structure may represent a continuation of the macro-anisotropic (dike) structure from the ZEV towards the east, with possibly modified geometrical and electrical properties. The following numerical simulations try to enlighten the quantitative aspects of this hypothesis.

Numerical modeling experiments

2-D regional modeling with anisotropy

In order to study the interaction between the mid-crustal conductor and a crustal anisotropic layer a series of 2-D numerical experiments were carried out based on the 2-D MT modeling algorithm for generally anisotropic structures (Pek and Verner, 1997). The principal aim of the modeling experiments was to analyze conditions under which the observed relation between the IV and the MT data can be reproduced on a regional scale.

As a regional conductivity background a slightly modified version of the model in Fig. 2 was used. The anisotropic structure in the Oberpfalz region is modeled by a 2-D E-W striking horizontally anisotropic block within the upper crust. This block extends over a 90 km long section of the crustal conductor in the southern part of the model, which corresponds to a broader area of the Saxothuringicum/Moldanubicum contact zone. The relatively large extent of the anisotropic structure was motivated by the fact that the high NW-SE to NNW-SSE (minor impedances) MT anisotropy is almost uniformly observed in all MT measurements carried out within the Moldanubian block west of the West Bohemian fault zone (Eisel, 1990), (Tauber, 1993), (Červ et al., 1997). Nevertheless, numerical simulations with the anisotropic block restricted to a more local crustal segment, roughly corresponding to the extent of the ZEV, were performed as well.

Two classes of 2-D anisotropic models were analyzed in detail. Models of the first class (left-hand

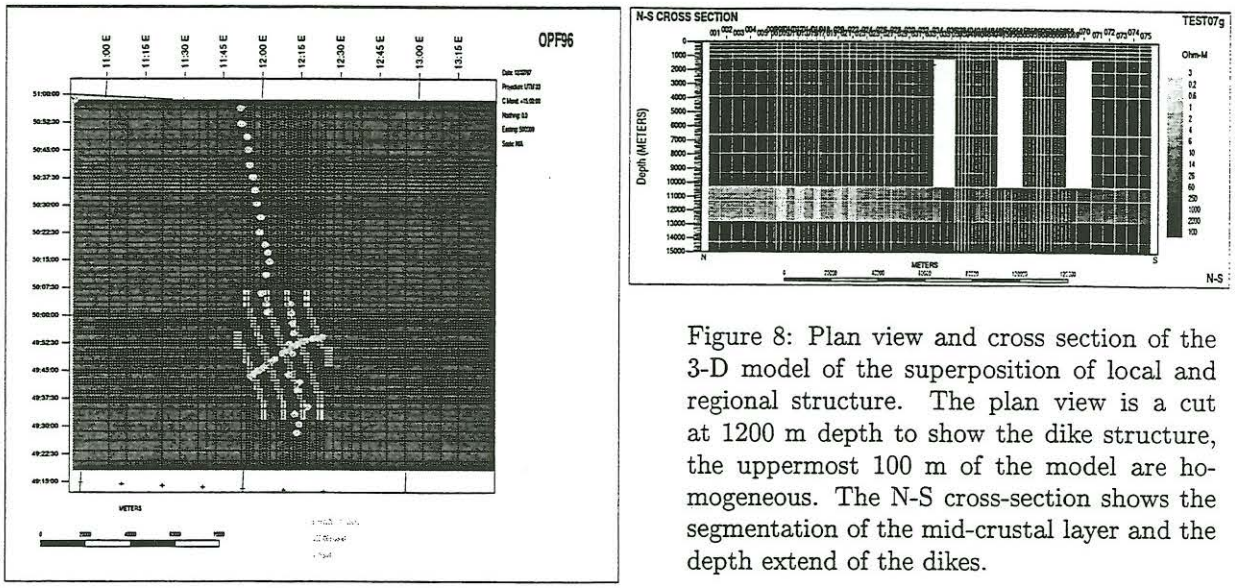

Figure 8: Plan view and cross section of the 3-D model of the superposition of local and regional structure. The plan view is a cut at 1200 m depth to show the dike structure, the uppermost 100 m of the model are homogeneous. The N-S cross-section shows the segmentation of the mid-crustal layer and the depth extend of the dikes.

panels in Fig. 7) are characterized by a superposition of the anisotropic block in the upper crust and the mid-crustal, E-W striking conductor. This type of models can qualitatively explain the relation between the direction of the IV and the magnetotelluric anisotropy. The anisotropy ratio within the block must be at least $\varrho_{min}/\varrho_{max} \sim 1/100$, and preferably even higher for keeping the MT anisotropy permanently large up to the longest periods involved. For smaller anisotropy ratios, the MT curves either do not reach the degree of anisotropy observed, or converge rapidly towards longer periods.

Two features of this model class are in disagreement with the observations: i) The limited N-S extend of the anisotropic block causes a deflection of the IVs in the boundary regions which is not seen in the field data. ii) The conductive layer causes a decrease in apparent resistivity of the yx component while the observed apparent resistivities of this component remain constant at high values.

The latter result restored the idea of a possible interruption or, at least, significant reduction of the regional E-W conductor below the area of interest, investigated already by Eisel (1995). This lead to the second class of 2-D anisotropic models with the anisotropic block penetrating into the deep conductive layer (Fig. 7, right-hand panels). This type of models is able to simulate the discrepancy between the magnetic and telluric directions, as well as the observed anisotropy of the MT curves. Moreover, the shape of the MT curves for the two perpendicular polarizations is reproduced more truly by this model. The anisotropy ratio within the deeper anisotropic block An2 must be at least $\varrho_{min}/\varrho_{max} \sim 1/100$ to produce the desired effect in the surface data, whereas the anisotropy of the upper crustal block An1 may be lower, about 1/30 or even less. The particular position of the top boundary of the highly anisotropic block affects mainly the period at which the splitting of the apparent resistivity curves starts.

3-D modeling with dike structures

A second approach to model the superposition of the regional mid-crustal conductor and the local anisotropic dike-structure was a full three-dimensional model. The 3-D finite difference code of Mackie (1993) was used for the model calculations. Fig. 8 shows a plan view and a N-S cross-section of the model. At 11 km depth the segmented conductor is incorporated, with slight modifications from the 2-D model in Fig. 2 in order to keep the size of the FD-mesh in reasonable dimensions. The dikes strike in an approximately NW-SE direction and reach to the top of the conductive layer. The topmost 1000 m of the model are homogeneous.

Fig. 9 compares apparent resistivities, phases, real IV and strike parameters from site SPA with those calculated for the corresponding model site. Both, the data from SPA and that from the model is rotated into a $N20°W$ coordinate system as indicated by the Swift angles. The general features of the data – anisotropy of the apparent resistivity, southward directed real IV at long periods and the strike direction are reproduced by the model data.

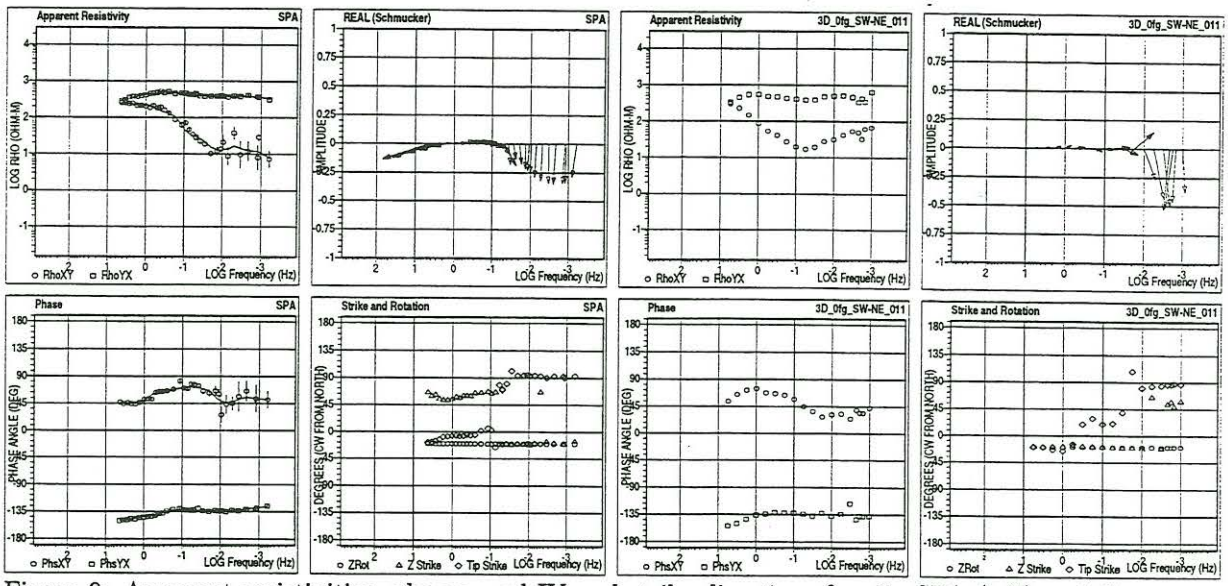

Figure 9: Apparent resistivities, phases, real IV and strike directions for site SPA (left) and the corresponding model site (right).

2-D local modeling of short-period induction arrows

The regional modeling experiments aimed mainly at explaining the regionally quasi-homogeneous relation between the IV and the MT anisotropy in the long-period range. Data for shorter periods, typically less than about 20 s, can provide further detailed information on the upper crustal electrical structure, but their interpretation is more difficult due to 3-D inhomogeneities. Therefore, the first modeling attempts with short-period data were restricted to the IV along the NE section of the profile. In this part of the profile, with only few exceptions, the IV seem to be consistently governed by crustal structures striking approximately N20°W (Fig. 5).

To model the structure, we used our 2-D E-polarization inversion procedure for models with variable geometry (Pek, 1987), and tried to fit both the real and imaginary part of the IV for four periods within the range 0.2 to 20 s (Fig. 10, panel B). Projections of the IV onto a line striking N73°E, which corresponds to the mean Swift's direction, were used as input to the inversion. Due to the known poor vertical resolution of the geomagnetic transfer functions, only two layers per column were reserved for the upper crustal segment between the overburden and the deep conductor, which is certainly an strong simplification.

The results of the inversion are presented in Fig. 10 where observed data and inversion results are compare ass functions of period and of profile location. These modeling experiments can be summarized as follows:

1. Most of the features of the IV can be explained by very shallow structures. This is true in particular for the peculiar reversal between SEU and GUM (see Fig. 5). Deeper conductors tend to influence a relatively large portion of the profile rather than to give a sharp and narrow reversal as observed in the experimental data. Surprisingly low, about 0.3 Ωm, is the interpreted resistivity of the shallow conductor between SEU and GUM. Its origin is not clear yet.

2. The rate of attenuation of the E-W IV for increasing periods, especially at SEU and GUM, requires the existence of a good conductor in the crust. The conductive layer at the depth of 10 km can produce the required damping effect provided its resistivity is a few Ωm only. For higher resistivities of this layer, the E-W reversal persists into the long-period range. This is demonstrated in panel C of Fig. 10 where the geomagnetic transfer functions at SEU and GUM are compared with the corresponding responses of two model versions, one with a well developed deep conductive layer ($\varrho_{CL} = 1.5$ Ωm) and the other with a moderately resistive layer ($\varrho_{NCL} = 300$ Ωm).

3. Even though MT data was not inverted, the principal features of the impedances can be reproduced by the present model with the deep conductive layer considered anisotropic with ϱ_{CL} along the strike

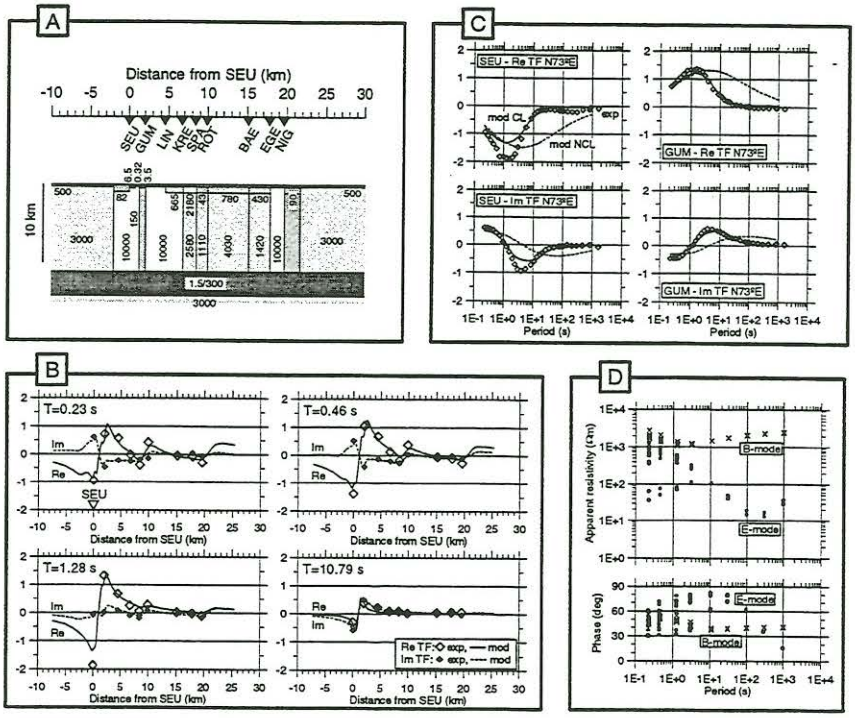

Figure 10: 2-D inversion model for short-period induction arrows along the NE section of the profile. The direction of the profile is N73°E. Panel A: Final 2-D model, with resistivities, in Ωm. A distance scale with site locations is shown above the model. B: Comparison of the experimental a model geomagnetic transfer functions, both real and imaginary, along the profile for four periods from the short-period range. C: Comparison of observed and modeled geomagnetic transfer functions (diamonds) for sites SEU and GUM and two model variants: CL (full line)–with highly conductive deep layer ($\varrho_{CL} = 1.5$ Ωm), and NCL (dashed line)–with only moderately increased conductivity of the deep layer ($\varrho_{NCL} = 300$ Ωm). D: E-mode (full circles, resistivity of the deep layer 1.5 Ωm) and B-mode (crosses, deep layer resistivity 300 Ωm) model apparent resistivities and phases for the model sites. All apparent resistivity curves are shifted to the respective median values at the period of 10 s.

and ϱ_{NCL} perpendicularly to it (Fig. 10, panel D). To eliminate the effect of irrelevant shifts, the apparent resistivities in the graph are shifted to their median value at 10 s.

Discussion and conclusion

The data collected along a 45 km SW-NE profile starting west of the FL, crossing the ZEV and ending in the region of Mariánské Lázně shows a clear improvement in data quality and therefore enables more detailed interpretations than could be achieved from existing MT data. Applying a multiple-station approach (Egbert, 1997) for the processing revealed the contamination of the data with strong coherent noise causing upward bias of the apparent resistivity curves which is not always immediately obvious. Refinements of the processing and a recognition scheme to locate undisturbed time segments yielded reliable estimates of MT impedances for most of the sites, though there is still some work necessary to get estimates for the easternmost sites.

The application of decomposition schemes reveals that most of the data is affected by three-dimensional geology rather than by distorted two-dimensional structures. This points to the direction which has to be chosen for the final interpretation: a full three-dimensional model.

The two-dimensional model studies, 2-D plus anisotropy for long period data on the one hand and 2-D inversion of IV for short period data on the other hand yield the pieces of the puzzle. The generalized three-dimensional superposition of the local and regional structure shows that the conductive layer at mid-crustal depth can obviously exist below the anisotropic upper crust – an answer to one of the questions posed to this experiment. The analysis of the data also revealed that the anisotropy extends further to the east, although the direction changes from NW-SE to NNW-SSE.

Acknowledgments

The field crew members Svetlana Byrdina, Jörg Beike, Patrick Denny, Thomas Verner, Oldrich Prous and Hassan El Shayeb made sure that this became a successful experiment even under toughest northeast Bavarian conditions. Gary Egbert's processing code and his thoughtful hints helped to finally get the coherent noise under control. This project is funded by the German Science Foundation (DFG, Ha1210/16-1). ME's stay at Oregon State University is supported under a grant from the German Academic Exchange Service (DAAD, Hochschulsonderprogramm III) and by the German Science Foundation (Ei370/4-1).

References

Bahr, K. (1991). Geological noise in magnetotelluric data: a classification of distortion types. *Phys. Earth Planet. Int.*, 66:24–38.

Červ, V., Pek, J., Pecova, J., and Praus, O. (1993 a). Electromagnetic measurements in the vicinity of the KTB drill site. Part I: The MV results across a 2-D array. *Studia geoph. et geod.*, 37:83–102.

Červ, V., Pek, J., Pecova, J., and Praus, O. (1993 b). Electromagnetic measurements in the vicinity of the KTB drill site. Part II: Magnetotelluric results. *Studia geoph. et geod.*, 37:168–188.

Červ, V., Pek, J., and Praus, O. (1997). The present state of art of long period magnetotellurics in the western part of the bohemian massif. *J. Geomag. Geoelectr.*, 49:1559–1583.

Egbert, G. D. (1997). Robust multiple-station magnetotelluric data processing. *Geoph. J. Int.*

Eisel, M. (1990). Über die Superposition von lokalen und regionalen Leitfähigkeitsanomalien, untersucht anhand magnetotellurischer Messungen entlang eines Nord-Süd-Profils im Nordosten der Oberpfalz. Diplomathesis, Inst. f. Meteorologie und Geophysik, J. W. Goethe-Univ. Frankfurt/Main.

Eisel, M. (1995). *Interpretation magnetotellurischer Messungen im Umfeld der Kontinentalen Tiefbohrung unter besonderer Berücksichtigung lateral anisotroper Leitfähigkeitsstrukturen.* PhD thesis, Freie Universität Berlin. published as Scientific Technical Report STR95/13 of the GeoForschungsZentrums Potsdam.

Eisel, M. and Haak, V. (1998). Macro-anisotropy of the electrical conductivity of the crust: A magnetotelluric study from the German Continental Deep Drilling site (KTB). *Geoph. J. Int.*

Groom, R. and Bailey, R. (1989). Decomposition of magnetotelluric impedance tensors in the presence of local three-dimensional galvanic distortion. *JGR*, 94, No. B:1913–1925.

Mackie, R. L., Madden, T. R., and Wannamaker, P. E. (1993). Three-dimensional magnetotelluric modelling using difference equations - theory and comparisons to integral equation solutions. *Geophysics*, 58:215–226.

Pek, J. (1987). Numerical inversion of the 2-D MT data by models with variable geometry. *Phys Earth Planet. Inter.*, 45:193–203.

Pek, J. and Verner, T. (1997). Finite-difference modelling of magnetotelluric fields in two-dimensional anisotropic media. *Geophys. J. Int.*, 128:505–521.

Siemon, B. (1991). *Ein Interpretationsverfahren für induktiv schwach gekoppelte Leitfähigkeitsanomalien, dargestellt am Beispiel des Salzstocks Wesendorf im Gifhorner Trog.* PhD thesis, Math.-Naturwiss. Fachbereiche, Univ. Göttingen.

Tauber, S. (1993). Die Leitfähigkeitsverteilung der nördlichen Varisziden untersucht mit der Methode der Magnetotellurik und der geomagnetischen Tiefensondierung auf einem Profil vom Oberpfälzer Wald ins Vogtland. Diplomarbeit, Institut für Geowissenschaften der Freien Universität Berlin.